Available online at www.sciencedirect.com
SCIENCE DIRECT®
Journal of Sound and Vibration 269 (2004) 765–780
JOURNAL OF SOUND AND VIBRATION
www.elsevier.com/locate/jsvi

Vibration control for an overhung roller in textile machine considering the stiffness of control device stand

Kazuki Mizutani[a,*], Kazumichi Kato[b], Takayoshi Fujii[b], Yili[a]

[a] *Department of Mechanical Engineering, Faculty of Engineering, Mie University, 1515 Kamihama-cho, Tsu, Mie 514-8507, Japan*

[b] *Research & Development Lab., Shinko Electric Co., Ltd., 100 Takegahana-cho, Ise, Mie 516-8550, Japan*

Received 5 June 2002; accepted 16 January 2003

Abstract

This paper treats a vibration control method that can be used in textile machinery to reduce the unbalanced vibration of an overhung roller–motor system. To control the vibration of the overhung roller, a drive motor with a hybrid type vibration control device consisted with rubber springs and electromagnets is used. When the vibration control system is set up in the textile machinery for industrial use, the stand supporting the control system to the base may be assumed not too rigid but elastic. For a certain value of the elastic stand stiffness, the vibration control performance of the overhung roller becomes very low. In order to prevent this deterioration, a stiffness control achieved by a positive feedback of the displacement signal of the rubber spring is proposed and the effectiveness of the stiffness control is confirmed by simulations and experiments.

1. Introduction

The development of high-speed and high-performance rotating machinery has focused on suppressing vibrations as a technological challenge. The vibrations of rotating machinery are mainly caused by either the static or dynamic unbalance of the rotor. The unbalance response of rotating machinery can be alleviated by a passive vibration control method such as a squeeze film damper [1,2] and a dynamic vibration absorber [3,4]. In order to effectively reduce the vibrations of rotating machinery, many active vibration control apparatus which use an electroviscous

*Corresponding author. Tel.: +81-59-231-9367; Fax: +81-59-231-9663.
E-mail addresses: mizutani@ss.mach.mie-u.ac.jp (K. Mizutani), kato-k@ise.shinko-elec.co.jp (K. Kato), fujii-t@ise.shinko-elec.co.jp (T. Fujii), yili@ss.mach.mie-u.ac.jp (Yili).

0022-460X/03/$ - see front matter
doi:10.1016/S0022-460X(03)00133-0

damper [5], piezoelectric actuator [6–9] and electromagnet [10–17] have been applied in recent years.

There are many types of rotating machinery with an overhung rotor, which is very sensitive to the rotor unbalance. It is difficult to control the vibrations of the overhung rotor directly, because the vibration control system may be hardly equipped on the overhung rotor, due to restrictions in the construction of the rotating machinery [6,7,14–17].

This paper describes a vibration control method that can be used in textile machinery to reduce the unbalanced vibration of an overhung roller–motor system. To control the vibrations of the overhung roller, we use a drive motor with a hybrid type vibration control device, in which the bearing housing of the motor is supported by rubber springs as a passive device and is installed in four pairs of electromagnets as an active device. The proportional and derivative (PD) control is performed in the active control system. The electromagnets give a control force to the bearing housing in the motor and effectively decrease the unbalanced vibration of the overhung roller. When the motor with the vibration control system is attached to industrial textile machinery, the stand supporting the motor to the foundation may be assumed not to be a rigid body but an elastic one. We consider the effect of the elasticity of the stand on the vibration control performance for the overhung roller, and show that the vibration suppression effect of the overhung roller becomes very low for a certain value of the spring constant of the elastic stand. We check the vibration control performance for many PD control parameters by numerical simulations, and obtain the proper condition of PD feedback gains to effectively control vibrations of the overhung roller.

The experimental results in our study are compared with the analytical ones, and both results show a similar tendency. We confirm that the hybrid type vibration control device in the drive motor is a highly effective device for the vibration suppression of the overhung roller system.

2. Experimental apparatus and analytical model

2.1. Experimental apparatus

Fig. 1 shows the schematic diagram of the experimental apparatus. This apparatus is a full-scale model that simulates a motor used in a product line of the textile industry. The mass of the overhung roller attached at the shaft end is 21.2 kg. The properties of the motor are 3.6 kW, 4-poles and 10 500 rotation/min in the rated speed. A hybrid type control device constructed of rubber springs and electromagnets is installed in the bearing pedestal on the anti-roller side. Two eddy current type displacement sensors are used to measure the displacements of the controllable bearing in the horizontal and vertical directions, respectively.

The attraction force generated by each pair of electromagnets f is shown by the following equation, in which the permeability in vacuum is μ_0, the area of a magnetic pole in the air-gap A_g, the number of turns of the coil N, the current in the coil i, and the air-gap distance δ:

$$f = \frac{\mu_0 A_g N^2}{4}\left(\frac{i}{\delta}\right)^2. \tag{1}$$

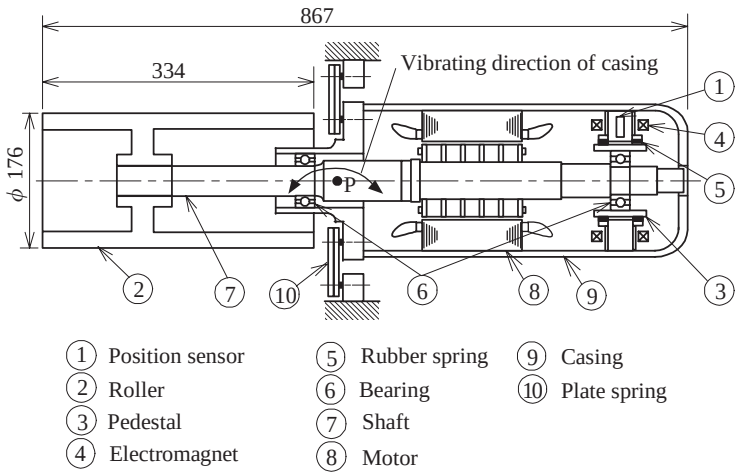

Fig. 1. Schematic diagram of experimental apparatus.

The magnetic force f in Eq. (1) has a non-linear characteristic that is inversely proportional to the square of the gap length and proportional to the square of the coil current. In order to linearize the magnetic force, two pairs of magnets are used to generate the push–pull magnetic force. Let the initial gap length be W_0, the variation of gap $\Delta\delta_n (n = 1, 2)$, the steady state coil current I_0 and the variation of the current $\Delta i_n\,(n = 1, 2)$. The push–pull magnetic force $f_n\,(n = 1, 2)$ is represented as in the following expression:

$$f_n = \frac{\mu_0 A_g N^2}{4}\left(\frac{I_0 + \Delta i_n}{W_0 + \Delta\delta_n}\right)^2 \quad (n = 1, 2). \tag{2}$$

The infinitesimal variation component near the equilibrium point $\Delta f_n\,(n = 1, 2)$ is obtained from Eq. (2) as follows:

$$\Delta f_n = 2F_0\left(\frac{\Delta i_n}{I_0} + \frac{\Delta\delta_n}{W_0}\right) \quad (n = 1, 2). \tag{3}$$

Here

$$F_0 = \frac{\mu_0 A_g N^2}{4}\left(\frac{I_0}{W_0}\right)^2.$$

Letting these two pairs of electromagnets be of the push–pull type, and denoting the relation between each coil current and the gap as $\Delta i_1 = -\Delta i_2 = \Delta i$, $\Delta\delta_1 = -\Delta\delta_2 = \Delta x$, the variation of the magnetic attraction force near the equilibrium point Δf is obtained as follows:

$$\Delta f = \Delta f_1 - \Delta f_2 = 4F_0\left(\frac{\Delta i}{I_0} + \frac{\Delta x}{W_0}\right). \tag{4}$$

The first term on the right-hand side of Eq. (4) represents the control force caused by the variation of the coil current Δi, and the second term represents the unstable force due to the negative stiffness of the electromagnet.

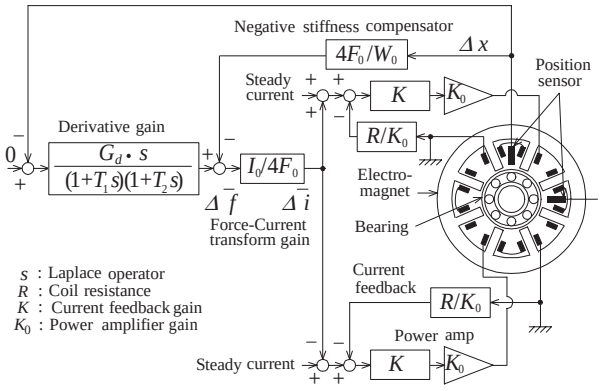

Fig. 2. Block diagram of control system.

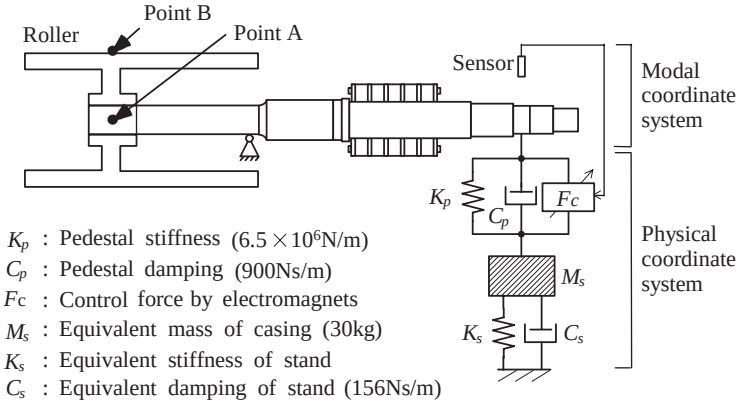

Fig. 3. Analytical model of roller–shaft system.

Fig. 2 shows the block diagram of the control system with a compensated circuit for a derivative control where G_d is a derivative gain. Because the coil current Δi becomes a first order time delay response to the current instruction $\Delta\bar{i}$, compensation with the current feedback is performed for the time delay, and negative stiffness compensation for the unstable force due to electromagnetic attraction is performed in this control circuit. In Fig. 2, a displacement of the flexible bearing is fed back to the derivative control circuit, and a damping force is applied to the bearing at the reverse side of the roller. To prevent noise and saturation in the higher frequency area, two steps of first order low pass filters (cut-off frequencies: $1/T_1 = 3.4\,\text{kHz}$ and $1/T_2 = 4.4\,\text{kHz}$) are interposed in the derivative circuit. The time constant of the coil is improved from 17.0 to 1.55 ms (cut-off frequency: 103 Hz) by the current negative feedback. The control is performed in the horizontal and vertical directions independently.

2.2. Analytical model

Fig. 3 shows an analytical model of the roller–shaft system, where the symbol F_c means the control force of the electromagnets, K_p and C_p mean the equivalent stiffness and the equivalent

damping coefficient of the flexible bearing pedestal, and M_s, K_s, and C_s are the equivalent mass, the equivalent stiffness, and the equivalent damping coefficient of the elastic stand, respectively. Since the boundary condition between the roller–shaft part and the control device changes with the magnitude of control forces, the model is divided into two components, one being the roller–shaft part, and the other the elastic stand parts with a control device. The analysis is performed by the Building Block method [18]. The roller–shaft part is represented by modal co-ordinates, and the elastic stand parts by physical co-ordinates. Using a modal method can reduce the dimension of roller–shaft part. A general form of the equations of motion for the roller–shaft part becomes as follows:

$$\mathbf{M}\ddot{\mathbf{z}} + \mathbf{C}\dot{\mathbf{z}} + \mathbf{K}\mathbf{z} = \mathbf{F}, \tag{5}$$

where $\mathbf{z} = \mathbf{x} + \mathrm{j}\mathbf{y}$, $\mathbf{F} = \mathbf{f}_\mathbf{x} + \mathrm{j}\mathbf{f}_\mathbf{y}$ ($\mathrm{j} = \sqrt{-1}$), the symbols $\mathbf{x}$ and $\mathbf{y}$ are node vectors, and $\mathbf{f}_\mathbf{x}$ and $\mathbf{f}_\mathbf{y}$ are external forces in the horizontal and vertical direction, respectively. The symbols $\mathbf{M}$ and $\mathbf{K}$ are a mass matrix and a stiffness matrix. The matrix $\mathbf{C}$ means a coefficient matrix regarding the damping and gyroscopic effects, and contains the damping and gyroscopic coefficients. In order to simplify the modal analysis, the damping and gyroscope effects of the overhung roller are neglected in the equations of motion (5). When the variable $\mathbf{z}$ in Eq. (5) is transformed to a modal displacement vector $\boldsymbol{\varphi}$ for the case $\mathbf{C} = 0$, the following equation is obtained:

$$\begin{bmatrix} \ddots & & \\ & m & \\ & & \ddots \end{bmatrix} \{\ddot{\boldsymbol{\varphi}}\} + \begin{bmatrix} \ddots & & \\ & k & \\ & & \ddots \end{bmatrix} \{\boldsymbol{\varphi}\} = \{\mathbf{F}_\varphi\}, \tag{6}$$

$$\{\mathbf{F}_\varphi\} = [\mathbf{N}]^\mathrm{T}\{\mathbf{F}\},$$

$$\mathbf{z} = [\mathbf{N}]\{\boldsymbol{\varphi}\},$$

where m, k and $\mathbf{N}$ are the modal mass, modal stiffness and vibration mode, respectively.

By assuming the symbol $\mathbf{z_m}$ to be the physical co-ordinate vector of the boundary parts of the support structure combined to the roller–shaft directly, and $\mathbf{z_r}$ to be the physical co-ordinate vector of the support structure except the vector $\mathbf{z_m}$, the equation of motion of the support structure is rewritten as follows:

$$\begin{bmatrix} \mathbf{M_{rr}} & \mathbf{0} \\ \mathbf{0} & \mathbf{M_{mm}} \end{bmatrix} \begin{Bmatrix} \ddot{\mathbf{z}}_\mathbf{r} \\ \ddot{\mathbf{z}}_\mathbf{m} \end{Bmatrix} + \begin{bmatrix} \mathbf{C_{rr}} & \mathbf{C_{rm}} \\ \mathbf{C_{mr}} & \mathbf{C_{mm}} \end{bmatrix} \begin{Bmatrix} \dot{\mathbf{z}}_\mathbf{r} \\ \dot{\mathbf{z}}_\mathbf{m} \end{Bmatrix} + \begin{bmatrix} \mathbf{K_{rr}} & \mathbf{K_{rm}} \\ \mathbf{K_{mr}} & \mathbf{K_{mm}} \end{bmatrix} \begin{Bmatrix} \mathbf{z}_\mathbf{r} \\ \mathbf{z}_\mathbf{m} \end{Bmatrix} = \begin{Bmatrix} \mathbf{F}_\mathbf{r} \\ \mathbf{F}_\mathbf{m} \end{Bmatrix}, \tag{7}$$

where $\mathbf{M}$, $\mathbf{C}$ and $\mathbf{K}$ with subscripts are the mass, damping and stiffness matrices of the support structure, respectively, and $\mathbf{F_m}$ and $\mathbf{F_r}$ are the control force and the external force applied at the

points $\mathbf{z_m}$ and $\mathbf{z_r}$, respectively. The combination of Eqs. (6) and (7) becomes as follows:

$$\begin{bmatrix} \begin{bmatrix} \ddots & & \\ & m & \\ & & \ddots \end{bmatrix} & \mathbf{0} & \mathbf{0} \\ \mathbf{0} & \mathbf{M_{rr}} & \mathbf{0} \\ \mathbf{0} & \mathbf{0} & \mathbf{M_{mm}} \end{bmatrix} \begin{Bmatrix} \ddot{\boldsymbol{\varphi}} \\ \ddot{\mathbf{z}}_\mathbf{r} \\ \ddot{\mathbf{z}}_\mathbf{m} \end{Bmatrix} + \begin{bmatrix} \mathbf{0} & \mathbf{0} & \mathbf{0} \\ \mathbf{0} & \mathbf{C_{rr}} & \mathbf{C_{rm}} \\ \mathbf{0} & \mathbf{C_{mr}} & \mathbf{C_{mm}} \end{bmatrix} \begin{Bmatrix} \dot{\boldsymbol{\varphi}} \\ \dot{\mathbf{z}}_\mathbf{r} \\ \dot{\mathbf{z}}_\mathbf{m} \end{Bmatrix}$$
$$+ \begin{bmatrix} \begin{bmatrix} \ddots & & \\ & k & \\ & & \ddots \end{bmatrix} & \mathbf{0} & \mathbf{0} \\ \mathbf{0} & \mathbf{K_{rr}} & \mathbf{K_{rm}} \\ \mathbf{0} & \mathbf{K_{mr}} & \mathbf{K_{mm}} \end{bmatrix} \begin{Bmatrix} \boldsymbol{\varphi} \\ \mathbf{z}_\mathbf{r} \\ \mathbf{z}_\mathbf{m} \end{Bmatrix} = \begin{Bmatrix} \mathbf{F}_\varphi \\ \mathbf{F}_\mathbf{r} \\ \mathbf{F}_\mathbf{m} \end{Bmatrix}. \tag{8}$$

The relation between the modal co-ordinate and the co-ordinate of the combined point is represented as in the following equation:

$$\{\mathbf{z_m}\} = [\mathbf{N}]\{\boldsymbol{\varphi}\}. \tag{9}$$

Using Eq. (9), the following relation is obtained.

$$\begin{Bmatrix} \boldsymbol{\varphi} \\ \mathbf{z}_\mathbf{r} \\ \mathbf{z}_\mathbf{m} \end{Bmatrix} = \begin{bmatrix} \mathbf{I} & \mathbf{0} \\ \mathbf{0} & \mathbf{I} \\ \mathbf{N} & \mathbf{0} \end{bmatrix} \begin{Bmatrix} \boldsymbol{\varphi} \\ \mathbf{z}_\mathbf{r} \end{Bmatrix}, \tag{10}$$

where $\mathbf{I}$ is a unit matrix. Substituting Eq. (10) into Eq. (8), and multiplying the transpose of the coefficients matrix from the left side, the final combined equation of the motion is derived as follows:

$$\begin{bmatrix} \begin{bmatrix} \ddots & & \\ & m & \\ & & \ddots \end{bmatrix} + \mathbf{N^T M_{mm} N} & \mathbf{0} \\ \mathbf{0} & \mathbf{M_{rr}} \end{bmatrix} \begin{Bmatrix} \ddot{\boldsymbol{\varphi}} \\ \ddot{\mathbf{z}}_\mathbf{r} \end{Bmatrix} + \begin{bmatrix} \mathbf{N^T C_{mm} N} & \mathbf{N^T C_{mr}} \\ \mathbf{C_{rm}} & \mathbf{C_{rr}} \end{bmatrix} \begin{Bmatrix} \dot{\boldsymbol{\varphi}} \\ \dot{\mathbf{z}}_\mathbf{r} \end{Bmatrix}$$
$$+ \begin{bmatrix} \begin{bmatrix} \ddots & & \\ & k & \\ & & \ddots \end{bmatrix} + \mathbf{N^T K_{mm} N} & \mathbf{N^T K_{mr}} \\ \mathbf{K_{rm} N} & \mathbf{K_{rr}} \end{bmatrix} \begin{Bmatrix} \boldsymbol{\varphi} \\ \mathbf{z}_\mathbf{r} \end{Bmatrix} = \begin{Bmatrix} \mathbf{F}_\varphi + \mathbf{N^T F_m} \\ \mathbf{F}_\mathbf{r} \end{Bmatrix}. \tag{11}$$

The compliances of the overhung roller are calculated from Eq. (11) by using the MATLAB/SIMULINK (The MATH WORK Inc.). A similar procedure is used when the damping and gyroscopic effects of the roller–shaft part are considered.

The rotating shaft is divided for each non-uniform section, and the mass and the moment of inertia for the roller and the rotor core of the motor are considered. The roller–shaft system is transformed into the mode co-ordinates by using the finite element method. The modes from first

to third are taken into account in this paper from the regions of the rotating speed and the controller frequency of the experimental apparatus. The equivalent mass M_s, stiffness K_s and damping coefficient C_s of the elastic stand are estimated from actual measurements. The equivalent damping coefficient of the rubber spring is also calculated from the damping ratio of the experimental result.

3. Analytical results

3.1. The relation between stand stiffness and vibration mode

Fig. 4 shows the calculated results of natural frequencies and vibration modes in the case of without control. Figs. 4(a)–(c) show the mode shapes for the spring coefficients of the elastic stand $K_s = 1.0 \times 10^6$, 1.6×10^7 and 8.0×10^7 N/m, respectively. The marks $\times$ in Fig. 4 show the vibration mode of the elastic stand M_s. The vibratory modes up to the third mode in Figs. 4(a) and (b) and only the first mode in Fig. 4(c) are included in the rated rotational speed of the experimental set-up, 10 500 rotation/min (167 Hz).

When the spring coefficient of the stand is relatively small like the one in Fig. 4(a), both the control force and the damping force of the rubber spring seem to have little effect on the vibration control for the first mode, because the relative displacement between the rotating shaft and the elastic stand (mark $\times$) becomes very small for this mode. In Fig. 4(b), the relative displacement between the rotating shaft and the elastic stand (mark $\times$) is almost zero for the second mode, and thus the damping control is less effective for this mode.

While the vibration control becomes possible for the other modes of Fig. 4, because the relative displacement between the rotating shaft and the elastic stand M_s is not equal to zero, the damping control is effective.

3.2. Damping control of controllably flexible bearing

When force is applied to the roller at point A shown in Fig. 3, the compliance of the roller system is obtained by numerical analysis. Fig. 5 shows the calculated results of the compliance of the roller at point A in Fig. 3 for the damping vibration control using the controllably flexible bearing. In this figure, the symbol C_e means the equivalent damping coefficient due to the derivative control that can be adjusted arbitrarily by varying the derivative gain G_d shown in Fig. 2. The spring coefficients of the stand are $K_s = 1.0 \times 10^6$, 1.6×10^7 and 8.0×10^7 N/m in Figs. 5(a)–(c), respectively. In Fig. 5, the dotted lines, solid lines, and dot-dash lines are for the case without control, $C_e = 2.0 \times 10^4$ and 1.0×10^5 Ns/m, respectively.

The compliance of the first mode hardly changes with the damping coefficient C_e for $K_s = 1.0 \times 10^6$ N/m in Fig. 5(a), because the rotating shaft and the elastic stand M_s move as one body, and the relative displacement becomes very small. For the second mode, the decreased relative displacement make the control impossible under the conditions of Fig. 5(b) for $K_s = 1.0 \times 10^7$ N/m. In Fig. 5(c) for $K_s = 8.0 \times 10^7$ N/m, the peak compliance of the second resonance becomes inconspicuous since the mode displacement of the roller becomes small at the second mode, and the relative displacement between the rotating shaft and the elastic stand is

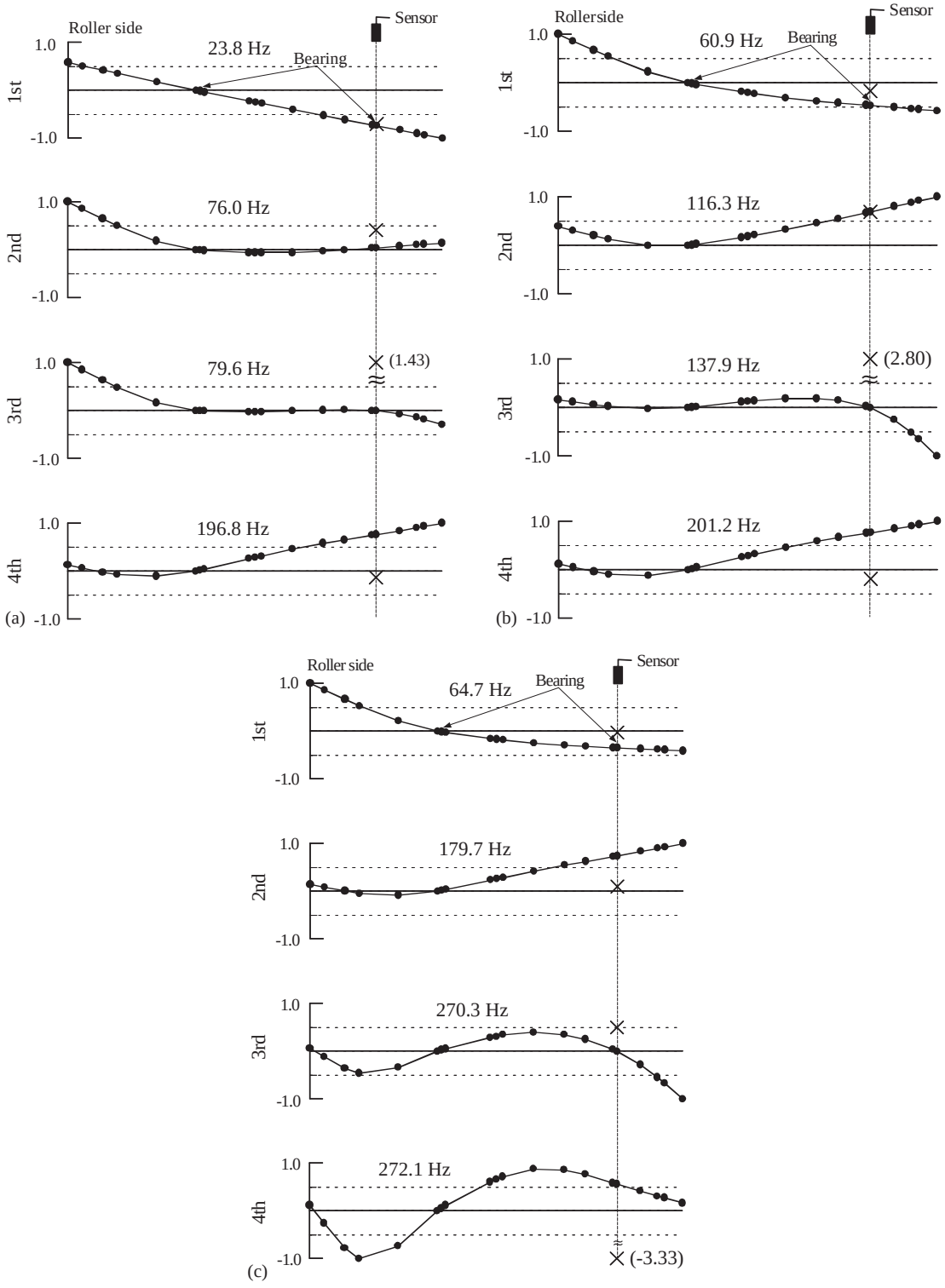

Fig. 4. Vibration modes without control (calculated results). (a) $K_s = 1.0 \times 10^6$ N/m, (b) $K_s = 1.6 \times 10^7$ N/m, (c) $K_s = 8.0 \times 10^7$ N/m.

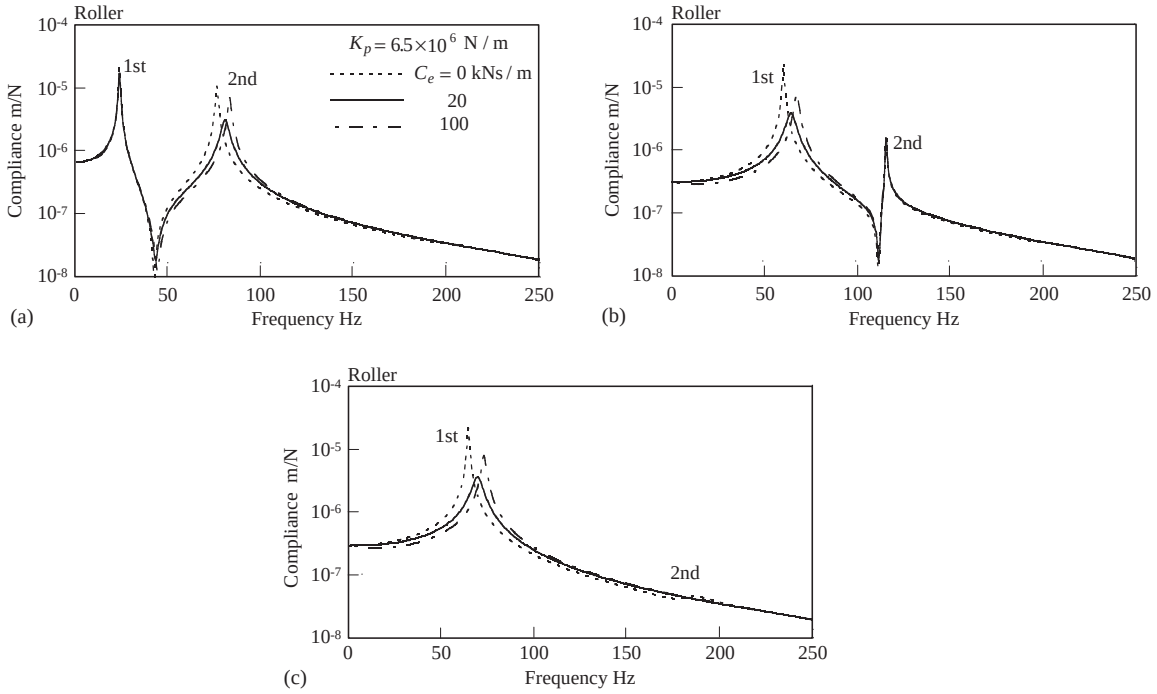

Fig. 5. Compliance of roller for damping control (calculated results). (a) $K_s = 1.0 \times 10^6$ N/m, (b) $K_s = 1.6 \times 10^7$ N/m, (c) $K_s = 8.0 \times 10^7$ N/m.

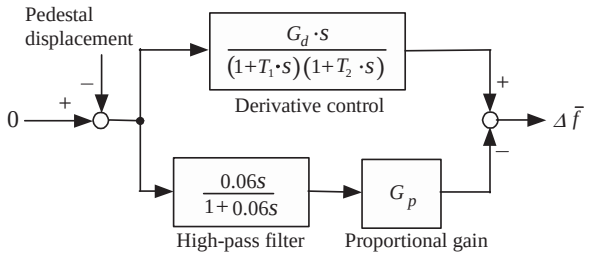

Fig. 6. Block diagram for stiffness control.

large, as shown in Fig. 4(c). In Fig. 5, the peak compliances of the first and second resonance become smallest for $C_e = 20$ kN s/m, and it can be concluded that there is an optimum value for the equivalent damping coefficient C_e.

3.3. Stiffness control of controllably flexible bearing

In Section 3.2, it is explained how the control effect to the vibration becomes less effective with the decrease of the relative displacement between the rotating shaft and the elastic stand M_s. The relative displacement depends on the flexural stiffness of the rotating shaft and the spring constants both of the rubber spring and the elastic stand. In order to perform the stiffness control,

the proportional gain block and a high-pass filter illustrated in Fig. 6 is added in the control loop shown in Fig. 2. The symbol G_p in Fig. 6 is the proportional gain. The stiffness control is achieved by conducting positive feedback of the displacement signal through a high-pass filter, and a proportional gain block in parallel with a derivative gain block. Since the positive feedback of the displacement signal of the flexible bearing is equivalent to the addition of a negative spring to the bearing pedestal, the stiffness control can be reduced to a spring constant, and the equivalent spring constant K_e due to the stiffness control becomes a negative value. Furthermore, by interposing a high-pass filter (the time constant: T_t), the reduction of stiffness in the lower frequency area can be prevented. The breaking frequency of the high-pass filter is equal to 2.65 Hz in order to neglect the effect of the first mode.

Fig. 7 shows the vibration mode for $K_s = 1.6 \times 10^7$ N/m and $K_e = -5.2 \times 10^6$ N/m, that is, $K_p + K_e = 1.3 \times 10^6$ N/m. In comparison with Fig. 4(b) for the same K_s value, the relative displacement between the rotating shaft and the elastic stand becomes larger, and an improvement of the effect on the vibration control is expected. The second mode is hardly improved, however, because this mode is determined by the values of M_s and K_s. Fig. 8 shows the calculated compliance of the roller at point A in Fig. 3 for the stiffness control. From Fig. 8, the peaks of compliance for the stiffness control are more obviously reduced than those for the damping control, except for the second mode in Fig. 8(b) for $K_s = 1.6 \times 10^7$ N/m.

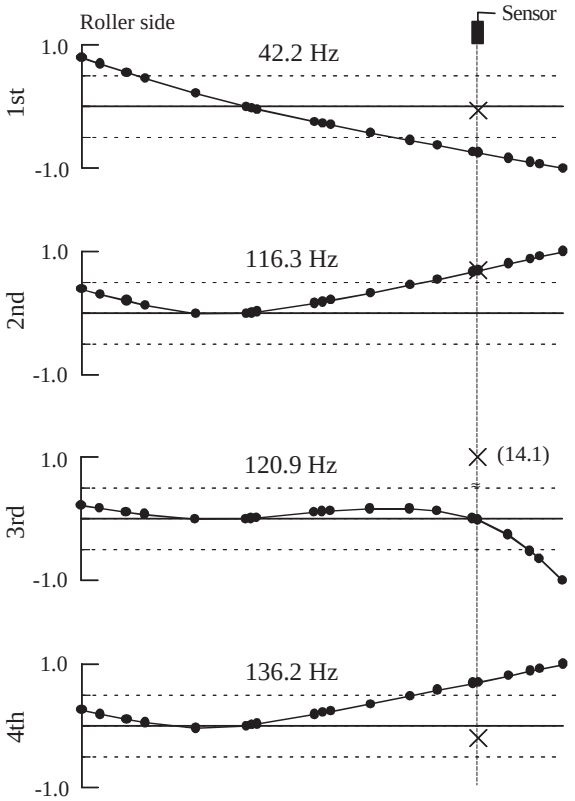

Fig. 7. Vibration modes with stiffness control (calculated results), $K_s = 1.6 \times 10^7$ N/m and $K_e = -5.2 \times 10^6$ N/m.

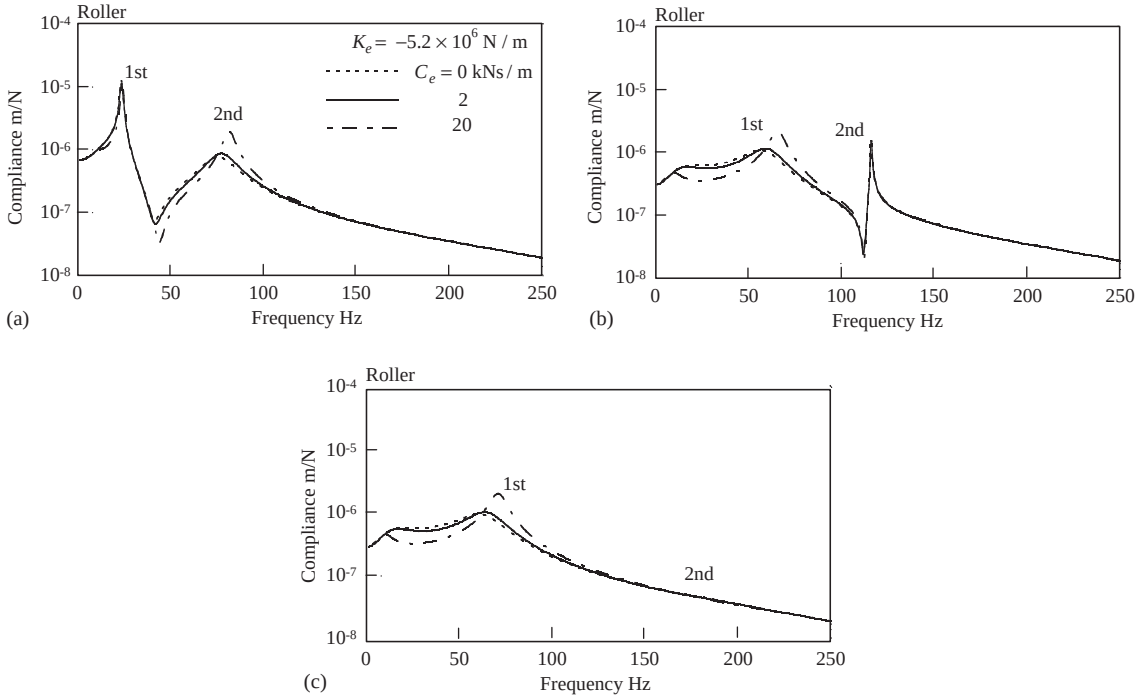

Fig. 8. Compliance of roller for stiffness control (calculated results). (a) $K_s = 1.0 \times 10^6$ N/m, (b) $K_s = 1.6 \times 10^7$ N/m, (c) $K_s = 8.0 \times 10^7$ N/m.

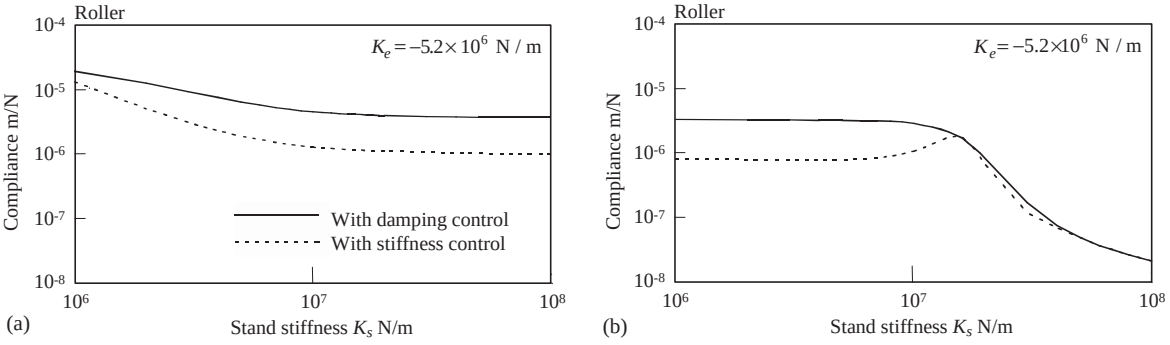

Fig. 9. Relation between stand stiffness K_s and peak compliance. (a) First resonance, (b) second resonance. The solid line indicates the damping control results ($K_e = 0$ N/m, $C_e = 20$ kN s/m) and the dotted line indicates the stiffness control results ($K_e = -5.2 \times 10^6$ N/m, $C_e = 0$ kN s/m).

Figs. 9(a) and (b) show the relations between the K_s value and the peak compliance at point A in Fig. 3 for the first and second modes, respectively. The solid line indicates the damping control results ($K_e = 0$ N/m, $C_e = 20$ kN s/m), and the dotted line indicates the stiffness control results ($K_e = -5.2 \times 10^6$ N/m, $C_e = 0$ kN s/m). The vibration control for the stiffness control is more

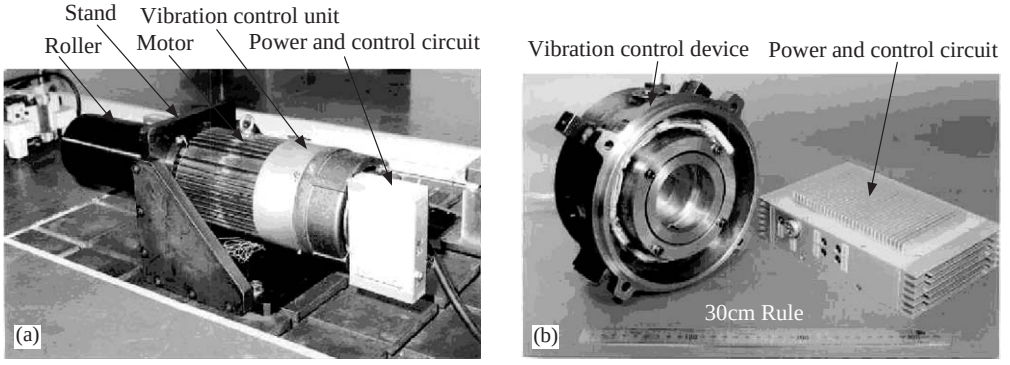

Fig. 10. (a) Photograph of experimental apparatus. (b) Photograph of vibration control device, and power and control circuit box.

effective than that for the damping control during all ranges of the stand stiffness at the first mode. But when K_s is greater than 1.6×10^7 N/m at the second mode, the compliance of the stiffness control is almost the same as that of the damping control.

4. Experimental results

The experiments are performed using the horizontal overhung roller system shown in Fig. 1. Figs. 10(a) and (b) present the photographs of the experimental apparatus, and vibration control device and control circuit box compared with a 30 cm rule.

The compliance is obtained by the transfer function between the striking force and the vibratory displacement when the roller is struck at point B on the outside of the roller in Fig. 3 by an impulse hammer. The measured natural frequencies without control are 24.0 Hz (first mode) and 77.5 Hz (second mode) for $K_s = 1.0 \times 10^6$ N/m, and 63.8 Hz (first) and 171 Hz (second) for $K_s = 8.0 \times 10^7$ N/m, which correspond to the calculation results of Fig. 4. Fig. 11 shows the roller compliance at point B in Fig. 3 with the damping control or the stiffness one for $K_s = 1.0 \times 10^6$, 1.2×10^7 and 8.0×10^7 N/m. Some K_s values differ a little from those in simulations because the spring constant of the stand can be only adjusted discontinuously in experiments. The experimental results agree well with the simulation results, and it is confirmed that the stiffness control is useful in practical machinery. For the case of stiffness control, a little peak appears near 10 Hz caused by the new root due to a high-pass filter. The tuning of K_e and C_e in the practical machine can also be easily adjusted only two gain controllers.

The unbalance responses of the roller at point B in Fig. 3 are shown in Fig. 12, which is obtained from the rotating experiments. Figs. 12(a) and (b) correspond to the stand stiffness $K_s = 1.0 \times 10^6$ and 8.0×10^7 N/m, respectively. The marks ○ represent the results of the damping control as the same condition as Figs. 5(a) and (c) for $C_e = 20$ kN s/m, and the marks ● represent those of the stiffness control for the same condition as Figs. 8(a) and (c) for $C_e = 0$ kN s/m. The effect of the stiffness control at the peak for the first and second modes is approximately similar to

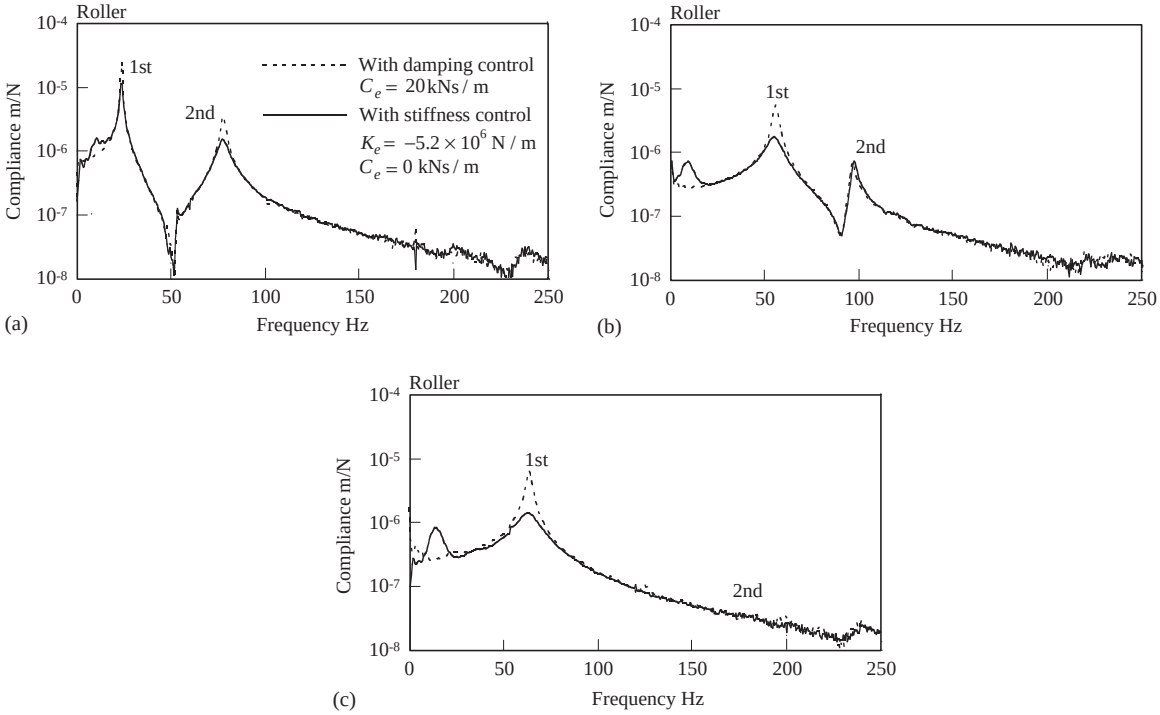

Fig. 11. Compliance of roller for damping and stiffness controls (experimental results). (a) $K_s = 1.0 \times 10^6$ N/m, (b) $K_s = 1.2 \times 10^7$ N/m, (c) $K_s = 8.0 \times 10^7$ N/m.

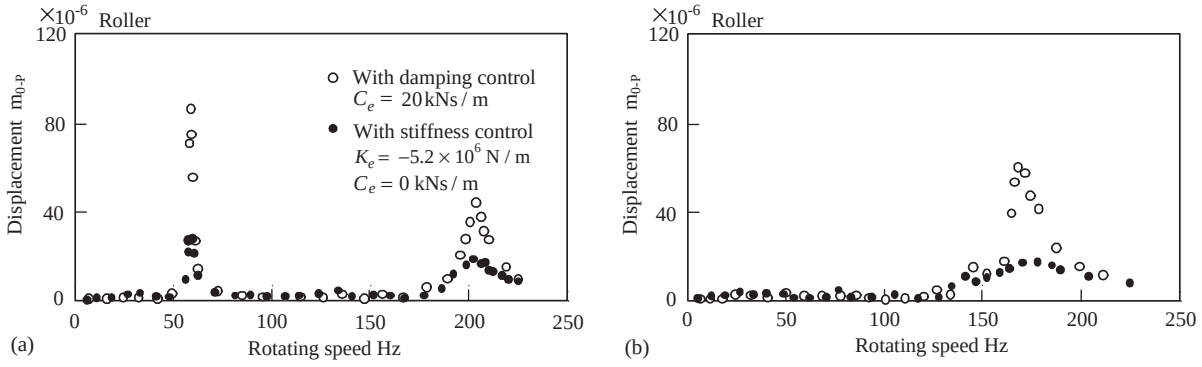

Fig. 12. Unbalance response obtained from rotating experiments. (a) $K_s = 1.0 \times 10^6$ N/m, (b) $K_s = 8.0 \times 10^7$ N/m.

the calculation results. It can be confirmed that the stiffness control is effective even for the unbalance responses. It is the main reason that the flexible bearing makes move easily because the equivalent spring constant of the flexible bearing is reduced for this positive feedback control, and then the vibration control forces, especially the damping control force, act on the overhung roller system more effectively.

5. Conclusions

In relation to the vibration control of the overhung roller–shaft system with the elastic stand proposed in this paper, the major results obtained are summarized as follows:

1. To control the vibration of an overhung roller–motor system used in textile machinery, a hybrid type vibration control device made with rubber springs as a passive device and electromagnets as an active device is proposed. For some conditions of the stand stiffness, the relative displacement from the flexible bearing to the elastic stand becomes very small, and thus the vibration control performance decreases.
2. In order to effectively control the vibration of the roller system with the elastic stand, the stiffness control achieved by the positive feedback of the displacement signal of the flexible bearing is applied, and simulations and experiments confirm the effectiveness of the stiffness control.
3. The calculations and the experiments are performed for a full-scale model used in a product line of the textile industry, and the results obtained in this paper can be applied in their entirety to the vibration control in practical machinery. The tuning of control gains in the practical machine can also be easily adjusted with only two gain controllers.

Appendix. A: Nomenclature

A_g	area of a magnetic pole in the air-gap
C_e	equivalent damping coefficient due to the derivative control
C_p	equivalent damping coefficient of the flexible bearing pedestal
C_s	equivalent damping coefficient of the elastic stand
f	attraction force generated by the electromagnet
f_1, f_2	push–pull magnetic force
F_c	control force of the electromagnet
G_d	derivative gain
G_p	proportional gain
i	current in the coil
I_0	steady state current in the coil
j	$=\sqrt{-1}$
k	modal stiffness
K_e	equivalent stiffness due to the stiffness control
K_p	equivalent stiffness of the flexible bearing pedestal
K_s	equivalent stiffness of the elastic stand
m	modal mass
M_s	equivalent mass of the elastic stand
N	number of coil turns
T_1, T_2	cut-off periods of low pass filter
T_t	time constant of high-pass filter
W_0	initial gap length of the magnet

δ	air-gap distance of the magnet
Δf	variation of magnetic attraction force from the equilibrium
Δf_1, Δf_2	variations of push–pull magnetic attraction forces from the equilibrium
Δi	variation of coil current from the equilibrium
$\Delta \bar{i}$	variation of instruction current from the equilibrium
Δi_1, Δi_2	variations of control current from the equilibrium
Δx	variation of gap of push–pull magnet from the equilibrium
$\Delta\delta_1$, $\Delta\delta_2$	variations of gap of push–pull magnet from the equilibrium
μ_0	permeability in vacuum

Vectors and matrices

$\mathbf{C}$	matrix contained damping coefficients and gyroscopic ones
$\mathbf{f_x}$	external force in the horizontal direction
$\mathbf{f_y}$	external force in the vertical direction
$\mathbf{F}$	$=\mathbf{f_x}+\mathrm{j}\mathbf{f_y}$
$\mathbf{F_m}$	control and/or external force applied at point $\mathbf{z_m}$
$\mathbf{F_r}$	control and/or external force applied at point $\mathbf{z_r}$
$\mathbf{I}$	unit matrix
$\mathbf{K}$	stiffness matrix
$\mathbf{M}$	mass matrix
$\mathbf{N}$	vibration mode
$\mathbf{x}$	node vector in the horizontal direction
$\mathbf{y}$	node vector in the vertical direction
$\mathbf{z}$	$=\mathbf{x}+\mathrm{j}\mathbf{y}$
$\mathbf{z_m}$	physical co-ordinate vector of boundary parts of the support structure combined to the roller–shaft
$\mathbf{z_r}$	physical co-ordinate vector of the support structure except $\mathbf{z_m}$
$\boldsymbol{\varphi}$	modal displacement vector

References

[1] A. El-Shafei, Stability analysis of intershaft squeeze film dampers, Journal of Sound and Vibration 148 (1991) 395–408.

[2] J.Y. Zhao, I.W. Linnett, L.J. Mclean, Unbalance response of a flexible rotor supported by a squeeze film damper, Transactions of the American Society of Mechanical Engineers, Journal of Vibration and Acoustics 120 (1998) 32–38.

[3] J.P. Den Hartog, Mechanical Vibrations, 4th Edition, McGraw-Hill, New York, 1956.

[4] K. Mizutani, K. Kato, K. Nakamura, Active vibration control of rotating shaft supported by flexible bearings, Proceedings of the IFToMM-jc, International Symposium on Theory of Machines and Mechanisms, Japan, 1992, pp. 526–531.

[5] J.L. Nikolajsen, M.S. Hoque, An electroviscous damper for rotor applications, Transactions of the American Society of Mechanical Engineers, Journal of Vibration and Acoustics 112 (1990) 440–443.

[6] A.B. Palazzolo, R.R. Lin, R.M. Alexander, A.F. Kascak, J. Montague, Piezoelectric pushers for active vibration control of rotating machinery, Transactions of the American Society of Mechanical Engineers, Journal of Vibration and Acoustics 111 (1989) 298–305.

[7] A.B. Palazzolo, R.R. Lin, R.M. Alexander, A.F. Kascak, J. Montague, Test and theory for piezoelectric actuator-active vibration control of rotating machinery, Transactions of the American Society of Mechanical Engineers, Journal of Vibration and Acoustics 113 (1991) 167–175.
[8] A.B. Palazzolo, S. Jagannathan, A.F. Kascak, G.T. Montague, L.J. Kiraly, Hybrid active vibration control of rotor bearing system using piezoelectric actuators, Transactions of the American Society of Mechanical Engineers, Journal of Vibration and Acoustics 115 (1993) 111–119.
[9] P. Tang, A. Palazzolo, A. Kascak, G. Montague, W. Li, Combined piezoelectric-hydraulic actuator based active vibration control for rotor–dynamic system, Transactions of the American Society of Mechanical Engineers, Journal of Vibration and Acoustics 117 (1995) 285–293.
[10] R. Stanway, J. O'Reilly, State-vibration feedback control of rotor-bearing suspension system, Proceedings of the Third International Conference on Vibration in Rotating Machinery, U.K., 1984, pp. 515–524.
[11] J.R. Salm, Active electromagnetic suspension of an elastic rotor: modeling, control and experimental results, Transactions of the American Society of Mechanical Engineers, Journal of Vibration, Acoustic, Stress, and Reliability in Design 110 (1988) 493–500.
[12] C.D. Bradfield, J.B. Roberts, S. Karunendiran, A programmable electromagnetic bearing for vibration control of a flexible shaft, Transactions of the American Society of Mechanical Engineers, Journal of Vibration and Acoustics 113 (1991) 160–166.
[13] C.W. Lee, J.S. Kim, Modal testing and suboptimal vibration control of flexible rotor bearing system by using a magnetic bearing, Transactions of the American Society of Mechanical Engineers, Journal of Dynamic, Systems, Measurement, and Control 114 (1992) 245–251.
[14] K. Mizutani, A. Asai, K. Kato, Control of unbalanced vibrations for a rotating machinery with an overhung rotor, Proceedings of the Asia-Pacific Vibration Conference, Korea, 1997, pp. 812–817.
[15] K. Kato, T. Fujii, K. Mizutani, Y. Kurita, Active vibration control of an overhung rotor system using electromagnets, Proceedings of the Asia-Pacific Vibration Conference, Korea, 1997, pp. 1234–1239.
[16] K. Mizutani, K. Kato, Vibration control for an overhung rotor system using actively flexible pedestal, Proceedings of the Asia-Pacific Vibration Conference, Singapore, 1999, pp. 472–477.
[17] K. Mizutani, Yili, R. Ikeura, Vibration control for an overhung rotor system considering the stiffness of control device mount, Proceedings of the Eighth International Congress on Sound and Vibration, Hong Kong, 2001, pp. 1841–1848.
[18] S. Murai, H. Ito, Y. Yoshioka, Dynamic design analysis of construction machinery, SAE Paper, No. 810924, 1981.